Suspended sediment transport at the instantaneous and event time scales in semiarid watersheds of southeastern Arizona, USA

Peng Gao,[1] Mark A. Nearing,[2] and Michael Commons[1]

Received 28 February 2013; revised 19 September 2013; accepted 23 September 2013.

[1] We investigated the high variability of suspended sediment transport in 16 watersheds of Walnut Gulch, southeastern Arizona, USA that were distinguished at three spatial scales: the plot (ca. 0.001–0.01 km^2), unit-source (ca. 0.01–0.1 km^2), and large (ca. 1–150 km^2) scales. Event-based data of water discharge and suspended sediment concentration were compiled in variable periods between the 1960s and 2010s. By subjectively distinguishing five different intraevent transport patterns that may be ascribed to a combination of various hydrological and sediment-transport processes, we showed that no single sediment rating curve could be developed for these data. However, at the event temporal scale, event specific sediment yield (SSY_e, t/km^2) was significantly correlated to event runoff depth (h, mm) for all transport patterns of the watersheds, suggesting that the complexity of suspended sediment transport at the intraevent scale is effectively reduced at the event scale regardless of watershed sizes. Further regression analysis indicated that the SSY_e-h relationship can be generally characterized by a proportional model, $SSY_e = nh$ where n, is conceptually equivalent to the volume-weighted event mean sediment concentration and is mainly determined by large events. For watersheds dominated by shrub cover, the change of the n value with watershed area was limited and thus may be reasonably regarded as a constant, implying that despite the highly variable suspended sediment concentrations during individual storm events in variable-sized watersheds, the synoptic effect of suspended sediment transport was similar and may be determined by a single value.

Citation: Gao, P., M. A. Nearing, and M. Commons (2013), Suspended sediment transport at the instantaneous and event time scales in semiarid watersheds of southeastern Arizona, USA, *Water Resour. Res.*, *49*, doi:10.1002/wrcr.20549.

1. Introduction

[2] Rates of soil erosion and sediment transport in arid and semiarid regions are highly variable both in space and over time [*Achite and Ouillon*, 2007; *Alexandrov et al*., 2009; *Mulligan*, 1998; *Nearing et al*., 2007; *Nichols*, 2006; *Zheng et al*., 2012]. This high variability is mainly due to the small-scale, temporally erratic nature of the rainfall events [*Coppus and Imeson*, 2002; *López-Tarazón et al*., 2010; *Martinez-Mena et al*., 2001]. Therefore, long-term observation is imperative to fully understand the dynamic controls of soil erosion and sediment transport [*Moran et al*., 2008; *Reid et al*., 1994].

[3] Using suspended sediment data collected over 10 years (1991–2001) in Nahal Eshtemoa, Israel, *Alexandrov et al*. [2007] demonstrated a relationship between suspended sediment concentration (*SSC*) and water discharge (Q) with a high degree of scatter. They argued that this poor *SSC*-Q relationship was primarily attributed to two different types of rainfall-runoff processes: convective storms prevailing in autumn that generally led to suspended sediment transport following clockwise loops; and frontal storms dominant in winter that tended to generate suspended sediment transport with anticlockwise loops. By separating the data in terms of these two different processes, better *SSC*-Q relationships were achieved, suggesting that processes of suspended sediment transport are different under the two different types of storms. *Achite and Ouillon* [2007] examined both instantaneous and daily-mean *SSC*-Q and sediment discharge, Q_s-Q power relationships using event-based data over 22 years in Wadi Abd watershed, Algeria. Although the instantaneous sediment rating curve varied greatly with the magnitudes of floods, the daily-mean *SSC*-Q relationship predicted sediment discharges reasonably well. They then demonstrated using this relationship that sediment load varied significantly among different seasons and years, which justifies continuous long-term sediment monitoring.

[4] *Zheng et al*. [2012] investigated the *SSC*-Q relationships over multiple temporal (instantaneous, event, and annual) and spatial (plot, subwatershed, and watershed) scales based on recorded data with the periods varying from 10 to 25 years in loess areas of northwestern China. Their analysis showed that there were no consistent instantaneous *SSC*-Q relationships persistent through all spatial scales. At the event scale, event mean sediment concentration

[1]Department of Geography, Syracuse University, Syracuse, New York, USA.
[2]USDA-ARS Southwest Watershed Research Center, Tucson, Arizona, USA.

Corresponding author: P. Gao, Department of Geography, Syracuse University, Syracuse, NY 13244, USA. (pegao@maxwell.syr.edu)

0043-1397/13/10.1002/wrcr.20549

calculated using data from large events changed greatly at the plot spatial scale and the degree of change reduced significantly as the spatial scale increased. At the annual scale, sediment yield was linearly correlated to runoff depth, while at the event scale it was proportional to runoff depth.

[5] *Polyakov et al*. [2010] calculated average annual precipitation, runoff and sediment yield over 34 years for eight small watersheds in southeastern Arizona. Their calculations showed that more than 50% of the total sediment yield of the study period was attributed to sediment yields generated by 10% of rainfall events, suggesting that the sediment yield was mainly produced by highly intensive storms. Yet, they found that the contribution of small events must be accounted for because of their high frequency of occurrence. Furthermore, they demonstrated that the long-term pattern of annual sediment yield cannot be solely explained by annual rainfall or large events, but is affected in a complex means involving many factors such as plant surface cover and rainfall timing.

[6] These studies, as well as the well-known hysteresis effect during storm events [*Bisantino et al*., 2011; *Fang et al*., 2008; *Gentile et al*., 2010; *Polyakov et al*., 2010] illustrated the ubiquitous complexity of interaction between sediment transport and storm patterns, topography, vegetation cover, and soil properties as spatial and temporal scales vary, and call for further continuous monitoring in order to understand environmental change such as global warming on dryland sediment transport. However, with currently available approaches and tools, future new data may provide limited information on suspended sediment transport. New insights into the complex sediment-transport processes are needed for developing new approaches to better understanding and managing sediment transport in arid and semiarid regions.

[7] This study aims to reveal the fundamental controls on sediment flux in semiarid watersheds by investigating patterns of suspended sediment transport at both instantaneous and event temporal scales and by developing a new event-based suspended sediment model that can quantify the general characteristics of long-term sediment dynamics and their spatial variations in a semiarid region of southeastern Arizona, USA. We first selected currently available long-term data from watersheds that belong to three physically based spatial scales in the study area. By examining the correlation between *SSC* (mg/l) and *Q* (m^3/s), and event specific sediment yield (SSY_e, t/km^2) and runoff depth (*h*, mm: total runoff volume normalized to watershed area), we showed that suspended sediment transport was complex at the intraevent temporal scale, but may well be characterized at the event temporal scale by statistically significant functions in terms of normalized runoff volume. Furthermore, we exhibited that these statistical functions can be reasonably replaced by a proportional model between SSY_e and *h*. We then explored the physical meaning of the model and provided an example for its application. The study was closed by showing the spatial variations of suspended sediment transport using the proportional model.

2. Methods

2.1. Classification of Spatial Scales

[8] Walnut Gulch Experimental Watershed (WGEW) is one of the two field sites operated by the Southwest Watershed Research Center (SWRC) of U.S. Department of Agriculture, Agricultural Research Service (USDA-ARS). It is located near Tombstone, Arizona, USA with the mean annual precipitation of 324 mm and the mean annual temperature of 17.6°C. Detailed description of geologic and geomorphological processes in, and physiographic conditions of WGEW may be found in *Osterkamp* [2008]. Within WGEW, 125 instrumented sites in a series of watersheds with different sizes have been monitored for hydrological and sediment data [*Nichols and Anson*, 2008; *Nichols et al*., 2008]. According to their geomorphological and hydrological characteristics, these watersheds can be generally divided into three different groups [*Kincaid et al*., 1966]. In watersheds of group one, specific processes of runoff movement and sediment transport may be isolated and identified. Watersheds in this group have small sizes, such that overland flow dominates hydrological and sediment-transport processes. Sediment yield is determined by rainfall (both amount and intensity), vegetation cover, surface ground cover, and microtopography [*Lane et al*., 1997]. The associated spatial scale is termed herein as *the plot scale*. Watersheds of group two have relatively homogeneous soil and vegetation cover with essentially uniform precipitation. In addition to hillslope processes, gully erosion and channel processes are also active. Hence, watershed sediment yields are not only influenced by hillslope processes, but also related to gully and alluvial channel densities and properties. These watersheds have been termed as unit-source watersheds [*Kincaid et al*., 1966; *Nearing et al*., 2007] and the associated spatial scale is herein referred to as *the unit-source scale*. In watersheds of group three, runoff movement and sediment transport are more controlled by complex in-channel hydraulics, while hillslope processes are still important [*Lane et al*., 1997]. The associated spatial scale is herein called as *the large scale*.

[9] Spatially, watersheds at the first two scales typically have areas less than 0.01 and between 0.01 and 0.1 km^2, respectively, whereas those at the third scale have areas between 1 and 150 km^2. Hydrologically, watersheds at the first two spatial scales have linear runoff (both volume and peak value) response to storms, while those at the large scale have nonlinear runoff response. The linear runoff response is ascribed to (1) uniform distribution and full cover of storms over watersheds because of their small areas and (2) less transmission loss through stream channels due to their relatively smaller areal sizes and depths. The nonlinear runoff response in those at the large scale is mainly caused by increased channel transmission loss and partial area storm coverage as watersheds increase in sizes [*Goodrich et al*., 1997]. Therefore, in watersheds at three different spatial scales, processes of suspended sediment transport have distinct characteristics.

2.2 Sampling Methods and Data Compilation

[10] Sampling instrumentation in the WGEW has improved since the initiation of sediment monitoring in 1960s and different sampling systems have been used in watersheds of different sizes because of equipment limitations and accounting for the variation of sediment sizes [*Nichols et al*., 2008]. At the plot scale, two watersheds, Flumes 105 and 106 have been monitored and event-based instantaneous suspended samples have been obtained using automatic pump samplers associated with H flumes

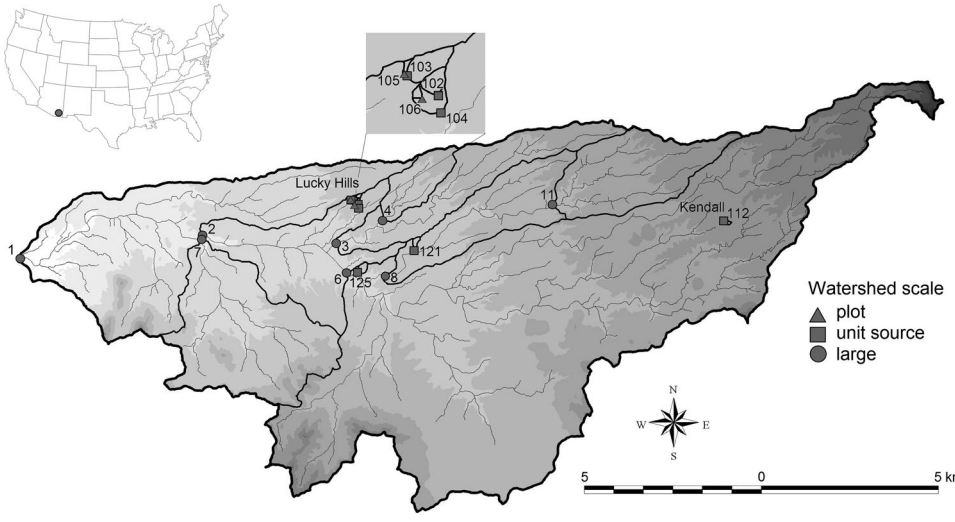

Figure 1. Sampling locations in Walnut Gulch Experimental Site, southeastern Arizona, USA.

[*Nearing et al*., 2007]. These two tiny watersheds do not have incised channels. Watershed 106 is nested within watershed 104 and watershed 105 drains into the channel immediately below Flume 103 (Figure 1). The available event-based instantaneous water discharge (Q) and suspended sediment concentration (SSC) data included 45 events spanning from 1996 to 2010 in Flume 105 and 59 events spanning from 1996 to 2011 in Flume 106, respectively (Table 1).

[11] At the unit-source scale, traversing slot sediment samplers have been used at the outlets of Flumes 102, 103, 104, 121, and 125, whereas an automatic pump sampler with a V-notch weir has been installed at the outlet of Flume 112. The first five watersheds are located in the Lucky Hills area (Figure 1), whose vegetation cover is dominated by a shrub plant community. These watersheds have well-developed channel systems and surface soils of sand-dominated mixture. Flume 112 is situated in a higher-elevated Kendall area (Figure 1) with vegetation cover dominated by grass and forbs. Its geomorphology is characterized by a swale (i.e., a flat valley bottom) that is seated above the outlet and serves as a sediment sink [*Nearing et al*., 2007]. The Q and SSC data available in these watersheds included 36–60 events spanning from 1995 to 2011 (Table 1). In watersheds at these two scales, data between 2005 and 2011 that were not used in Nearing *et al*. [2007] were included here along with the data before 2005. Thus, data listed in Table 1 represent the longest series of Q-SSC pairs available for these watersheds.

[12] At the large scale, Q and SSC data were obtained using V-notch weirs and automatic pump samplers with a depth-integrating sampling tube, respectively [*Simanton et al*., 1993]. Because of safety concerns and resources required in sampling these main channels, the sediment sampling program ended in the early 1980s [*Nichols et al*., 2008]. Thus, the Q and SSC data were only available between 1964 and 1975 in eight watersheds (Table 1). Although in Flumes 4, 7, 8, and 11, the data only contained seven or eight events, these events represent storms with a wide range of amount and intensity that produced diverse event runoff depths. Data in Flume 3 were mainly recorded during relatively small storm events. Despite this bias, we included these data to reflect the diversity of sediment-transport processes at this spatial scale. These watersheds have a wide range of areas (from 2.27 to 149.33 km^2) and form two nested watershed sequences in the descending order: Flumes 1, 2, 6, 3, and 4; Flumes 1, 2, 6, 8, and 11 (Figure 1).

2.3. Data Analysis

[13] Instantaneous values of Q and SSC for a given event have been commonly described using hysteresis analysis [*Gao*, 2008; *Oeurng et al*., 2010; *Smith and Dragovich*, 2009]. Although different patterns of hysteresis loops may be related to different transport processes, these links are essentially qualitative and hence have limited ability of characterizing dynamic sediment-transport processes. For example, a clockwise loop may reflect the dominance of in-stream sediment transport [*Gao and Josefson*, 2012; *Jansson*, 2002], but may also be the result of sediment transport on hillslope in small watersheds [*Lefrancois et al*., 2007; *Sadeghi et al*., 2008]. To better understand the dynamic patterns of instantaneous suspended sediment transport, we combined hysteresis analysis with the examination of coupled patterns between hydrograph and sedigraph for all individual events. First, we subjectively identified five different patterns in terms of Q and SSC variations during the rising and falling limbs, and their relative values toward the beginning and end of an event. The differences among these five patterns were not determined statistically, but physically. As a result, in some watersheds, a given pattern may have only one or no event. Because the purpose of distinguishing these patterns is to show the complexity of suspended sediment transport at the intraevent time scale, the subjectivity in determination of the classes does not undermine their capacity of achieving the purpose. Second, we link these patterns to typical hysteresis loops to identify the possible physical processes controlling suspended sediment transport.

[14] To examine sediment-transport behavior at the event temporal scale, we calculated event sediment yield (SSY_e, t/km^2) and runoff depth (h, mm) based on instantaneous Q and SSC data of each event and performed

Table 1. Information of the Selected Data and Event Distributions in Five Subjective Patterns for All Selected Watersheds

Watersheds	A (km^2)	Range of Data	No. of Events	Pattern One	Pattern Two	Pattern Three	Pattern Four	Pattern Five
				The plot scale				
Flume 105	0.0018	1996–2010	45	29	3	1	7	5
Flume 106	0.0034	1996–2011	59	41	6	1	4	7
				The unit-source scale				
Flume 102	0.0146	1998–2011	36	10	3[a]	11	7	5
Flume 103	0.0368	1995–2011	60	25	1	16	17	1
Flume 104	0.0453	1996–2011	51	17	3[b]	17	10	5
Flume 121	0.0542	1995–2011	57	20	9[c]	12	13	5
Flume 125	0.0591	1996–2011	40	13	8	4	11	1
Flume 112	0.0186	1995–2010	39	10	3	2	6	4
				The large scale				
Flume 1	149.33	1964–1975	75	24	18	2	7	24
Flume 2	113.72	1964–1974	22	6	11	0	0	5
Flume 3	8.98	1964–1974	7	0	2	1	0	4
Flume 4	2.27	1964–1974	8	3	0	1	1	3
Flume 6	95.1	1964–1975	102	32	22	6	10	32
Flume 7	13.52	1968–1974	7	1	1	1	1	3
Flume 8	15.5	1964–1973	8	3	0	0	0	5
Flume 11	8.24	1968–1974	8	0	0	0	2	6

[a]All the three events had constant *SSC* values.
[b]One had constant *SSC* values.
[c]Two of them had constant *SSC* values.

regression analysis to obtain the best-fit SSY_e-h relationship for each watershed. By comparing the predictions of the best-fit SSY_e-h relationship with those of three other different mathematical functions, we demonstrated that the proportional function may replace the best-fit SSY_e-h relationship for all watersheds and is indeed a general model for characterizing the SSY_e-h relationship. We subsequently provided mathematical and geomorphological explanations of the general model and then used it to reveal the general nature of the processes controlling suspended sediment transport through multiple spatial scales.

3. Results and Analysis

3.1. Watersheds at the Plot Spatial Scale

3.1.1. Variable Transport Patterns at the Intraevent Temporal Scale

[15] The 45 events of Flume 105 were divided into five patterns in terms of their hydrological and sediment-transport characteristics. In the first pattern, which contains 29 events (Table 1), *SSC* was (relatively) high at the beginning of the event and gradually decreased as Q increased during the rising limb of the event. The *SSC* value consistently decreased as Q decreased during the falling limb (Figure 2a). The decrease of *SSC* values was not controlled by Q variation, but by the availability of sediment within the watershed, demonstrating an apparent "depletion" effect. In pattern two, which included three events, the variation of *SSC* was in phase with that of Q (Figure 2b), suggesting that sediment transport in these events was primarily controlled by Q. Pattern three only contained one event, in which *SSC* increased continuously from the beginning to the end of the event, indicating ample sediment supply particularly toward the end of the event (Figure 2c). The seven events in pattern four showed different degrees of the depletion effect. For example, during the 12 July 1996 event, the *SSC* value of the first point was higher than that of the last two points, though the Q value of the first point was lower than those of the last two points (Figure 2d). This seems to suggest that less sediment was available during the falling limb than the rising limb. Data in each of the five events in pattern five only represented partial event duration (Figure 2e). Thus, these events cannot be classified into any one of the previous four patterns, though they still may be used to calculate SSY_e and h.

[16] Although events in patterns one and four showed different degrees of the depletion effect, the former were dominated by clockwise loops, while the latter were controlled by anticlockwise figure-8 loops [*Williams*, 1989]. The pattern-three event was dominated by an anticlockwise loop, whereas the pattern-two events tended to be controlled by weak loops, such that the data points of each event may be reasonably well characterized by a sediment rating curve. The diverse hysteresis types of sediment transport distinguish the small, semiarid watersheds from their humid counterparts in which intraevent sediment transport is generally controlled by clockwise loops [*Langlois et al*., 2005; *Lefrancois et al*., 2007; *Sadeghi et al*., 2008; *Seeger et al*., 2004; *Smith and Dragovich*, 2009] because sediment eroded from hillslope can be quickly transported to the watershed outlets and hillslope sediment supply is limited. These hysteresis types reflect the complex interaction of four main factors at this spatial scale: rainfall (both intensity and amount), vegetation cover, surface ground cover (including soil and rock fragment sizes), and topography (and its spatial variation) [*Lane et al*., 1997].

[17] Nonetheless, the depletion effect exhibited at this spatial scale should not be explained as the result of progressive seasonal exhaustion of sediment [*Thomas et al*., 2004] because many events were recorded in summer when sufficient erodible colluvium was available. Our in situ

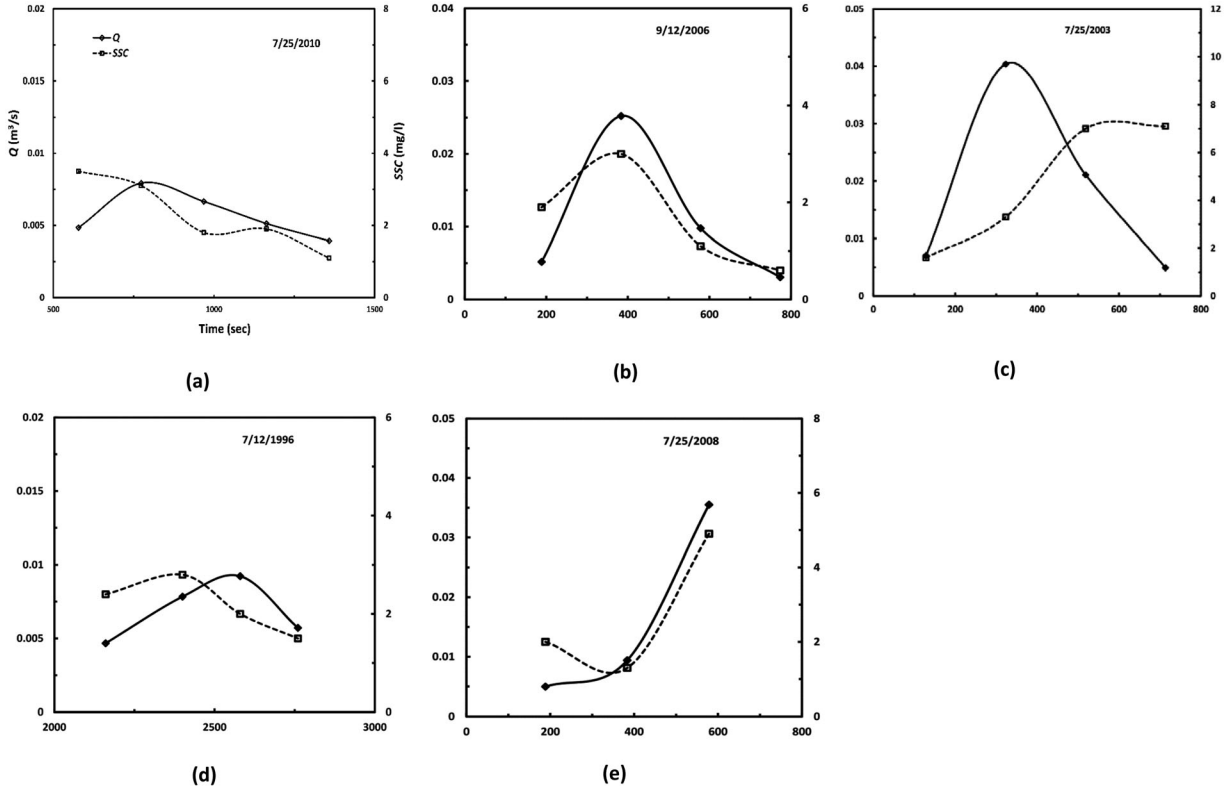

Figure 2. Examples of five intraevent transport patterns identified for Flume 105. (a) Pattern one; (b) pattern two; (c) pattern three; (d) pattern four; (e) pattern five.

observation indicated that this effect was most possibly caused by the relatively more sediment supply at the beginning of an event due to the availability of deposited sediment from the previous event. The sediment exhaustion was further enhanced by the following two processes commonly active in the study area. First, watersheds are dominated by heterogeneous gravelly sand (52%) [*Nearing et al*., 2007]. Hence, selective sediment detachment by raindrop and selective sediment transport by runoff lead to limited sediment transport [*Issa et al*., 2006; *Parsons et al*., 1991]. Second, surface crust due to the compression of soil surface or the depression of fine particles in pore spaces limits soil erosion [*Romkens et al*., 1990], causing decreased sediment-transport rates toward the end of an event [*Turnbull et al*., 2010].

[18] The existence of patterns two and three suggests that processes other than selective and limited sediment transport also influenced transport processes, making dynamics of sediment movement complex. However, these events only took 10% of the total recorded full events, which indicates that the impact of these other processes on suspended sediment transport was limited. Because all 45 events were collected between June and October when precipitation is predominately generated by convective storms [*Goodrich et al*., 2008], the prevalence of events with clockwise loops (>70%) seems to be related to this type of storms, which is consistent with the discovery reported in a semiarid watershed of Israel [*Alexandrov et al*., 2007]. Unfortunately, no single sediment rating curve was able to be established to characterize intraevent sediment transport (Figure 3a).

[19] The 59 events of Flume 106 can also be divided into these five patterns with 41 in pattern one, 6 in pattern two, 1 in pattern three, 4 in pattern four, and 7 in pattern five (Table 1). Although events in patterns one and four generally showed the depletion effect, processes other than the previously described could still contribute to this effect. For example, two events in pattern one (Figures 4a and 4b) had similar runoff depths (9.40 mm for the 14 July 1999 event and 9.45 mm for the 25 July 2010 event), but significantly different event specific sediment yield ($SSY_e = 58.43$ and 26.45 t/km^2, respectively). Examining the data indicated that the first event had greater peak rainfall intensity than that of the second, giving rising to the peak discharge $Q_p = 0.075$ m^3/s and peak concentration $C_p = 11.7$ mg/l for the first event and 0.024 m^3/s and 7.7 mg/l for the second. Furthermore, rainfall duration of the first one was much longer than that of the second. Thus, though the two different rainfall patterns produced similar runoff depth, their intraevent surface runoff patterns and changes were quite different, causing different event sediment yields. It follows that even within the same pattern, sediment-transport processes could be quite different because of variable storm intensity and duration. In all recorded full events, 87% had clockwise loops, which again indicated the dominant impact of convective storms on suspended sediment transport. The scatter plot of *SSC* against *Q* for Flume 106 is similar to that for Flume 105 (i.e., Figure 3a), again signifying that no single sediment rating curve was available for characterizing the instantaneous *SSC*-*Q* relationship in this watershed.

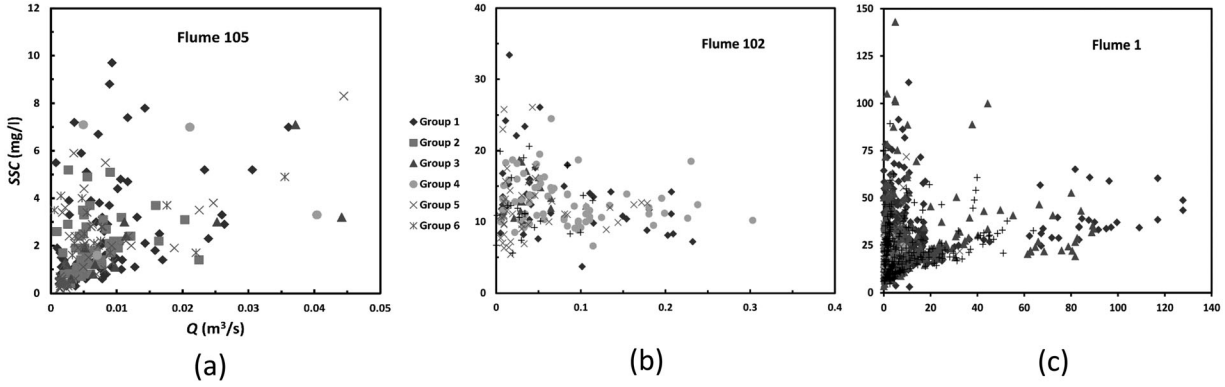

Figure 3. Scatter plots of suspended sediment concentration (*SSC*) versus water discharge (*Q*) at three spatial scales. (a) The plot scale; (b) the unit-source scale; (c) the large scale.

3.1.2. Sediment-Transport Processes at the Event Temporal Scale

[20] The complex sediment-transport processes described for the plot-scale watersheds indicate that developing general sediment rating curves even for a single watershed was impossible. Alternatively, we focused on the synoptic effect of sediment transport at the event temporal scale by examining the relationship between SSY_e and h. In Flume 105, data representing events in all five patterns collapsed well into a single trend with some events in pattern two showing relatively higher discrepancy (Figure 5a). The well-mixed trend among different patterns suggests that the synoptic effects of suspended sediment transport among all groups are similar. This trend was best characterized by a second-order polynomial equation:

$$SSY_e = 0.175h^2 + 2.074h + 0.003 \quad r^2 = 0.78 \qquad (1)$$

[21] The general good fit of equation (1) to the data (relatively high coefficient of determination, r^2) suggests that though sediment transport in the events of different patterns was dominated by different processes, the difference had a statistically insignificant impact on the SSY_e-h relationship. Therefore, from the instantaneous to event temporal scale, complex sediment dynamics during individual events are simplified, such that values of SSY_e of all events may be simply estimated by their runoff depths, h using a single empirical equation (i.e., equation (1)).

[22] In Flume 106, some events in patterns one, two, three, and five were apparently separated from others (Figure 5b). However, regression analysis showed that all events may be fitted well by a statistically significant second-order polynomial equation:

$$SSY_e = 0.028h^2 + 3.1h - 0.47 \quad r^2 = 0.80 \qquad (2)$$

[23] The sum of SSY_e for all events predicted using equation (2) was only 3% less than that of measured SSY_e. This again suggests that at the event temporal scale, event sediment yield (SSY_e) may be reasonably well characterized using equation (2).

3.2. Watersheds at the Unit-Source Spatial Scale

3.2.1. Variable Transport Patterns at the Intraevent Temporal Scale

[24] The storm events recorded in these watersheds also fell into the five patterns described in the plot-scale

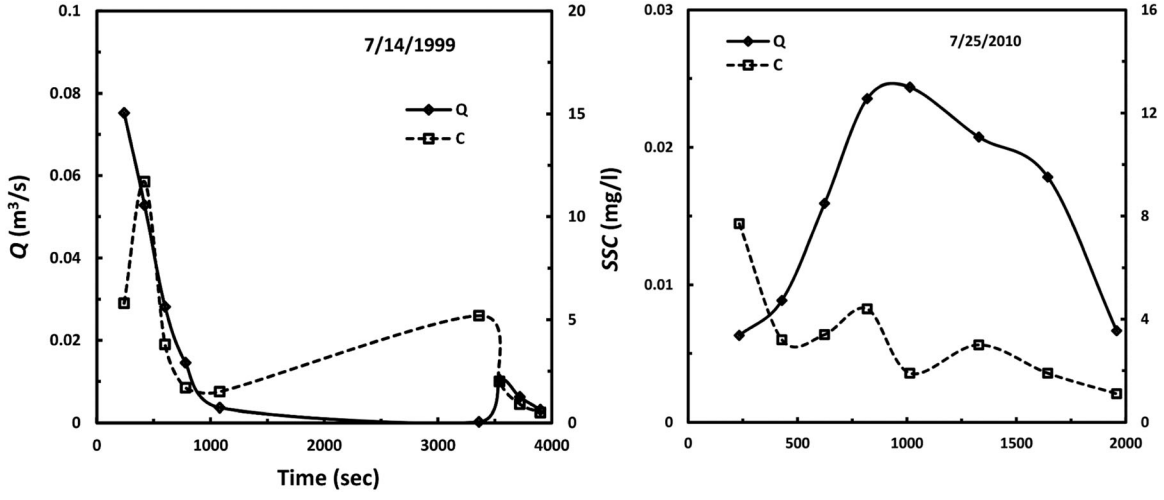

Figure 4. Two events of pattern one in Flume 106 that have similar runoff depths but different event specific sediment yields.

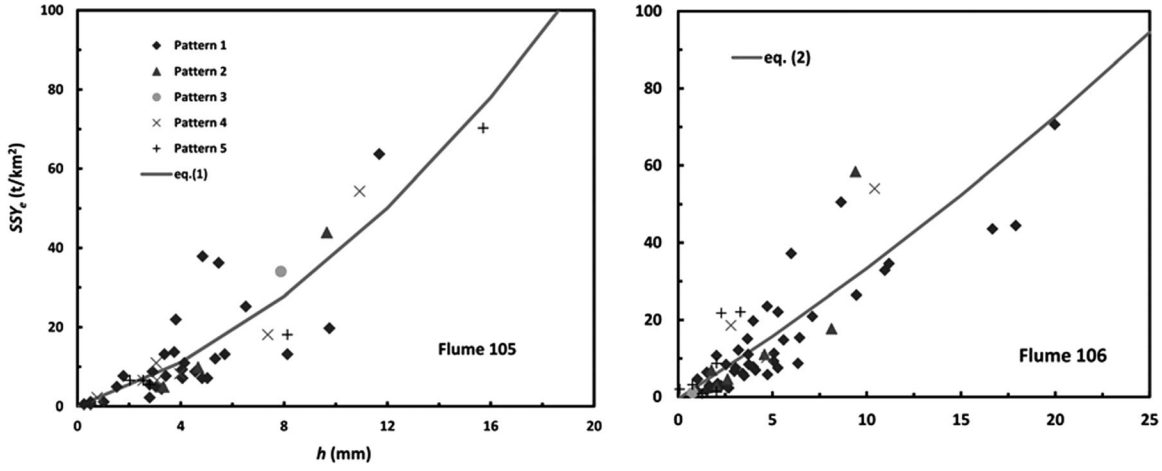

Figure 5. The relationships between event specific sediment yield (SSY_e) and runoff depth (h) for (a) Flume 105 and (b) Flume 106.

watersheds with some variations. The exact styles of individual events in patterns one, three, and four may be different from, but shared the common transport nature with those in the plot-scale watersheds. Certain events of pattern two in some watersheds (i.e., Flumes 102, 112, and 121) bore a different pattern from that of the events in the plot-scale watersheds. Instead of having approximately synchronized Q_p and C_p, these events were characterized by roughly constant *SSC* values over the entire storm duration (Figure 6), suggesting that the rate of transported sediment changed proportionally with Q. If soils available for transport by surface runoff were sufficient, *SSC* values during the events would be higher for large Q values than those for small ones, leading to discernible variation of *SSC* values over an event. Apparently, surface soils during these constant-*SSC* events were constrained as described previously, but the degree of the constraint was lower than that for events in patterns one and four where *SSC* values toward the end of the events were lower than those close to the beginning of the events. The detailed distributions of the events in the five patterns for these watersheds were displayed in Table 1.

[25] Among all events in the five patterns, those in patterns one and four showed various degrees of the depletion effect, while those in pattern three demonstrated the transport processes with sufficient sediment supply. Events with constant *SSC* in pattern two belonged to the former, while others in the same pattern were associated with the latter. It follows that the percentage of events that had the depletion effect in these six watersheds was (in the order shown in Table 1) 65%, 71%, 60%, 63%, 74%, and 94%, respectively. Again, events with the depletion effect prevailed in all watersheds at this spatial scale, though in-channel hydraulic processes added additional influence on suspended sediment transport due to the existence of ephemeral streams in these watersheds. The processes controlling instantaneous suspended sediment transport were still complex at the unit-source spatial scale, such that no single sediment rating curve was available for describing the *SSC*-*Q* relationship (Figure 3b).

3.2.2. Sediment-Transport Processes at the Event Temporal Scale

[26] In all watersheds, points representing events of all five patterns were well mixed and followed a single trend in the plot of SSY_e against h (Figure 7), suggesting that they also may be described by a single relationship. Regression analysis showed that this relationship was best fitted by second-order polynomial equations:

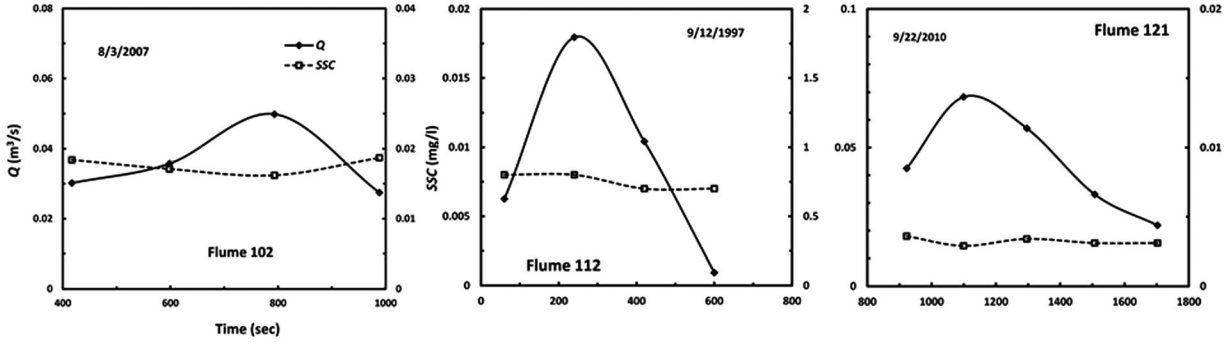

Figure 6. Examples of constant sediment concentrations in pattern-two watersheds at the unit-source scale.

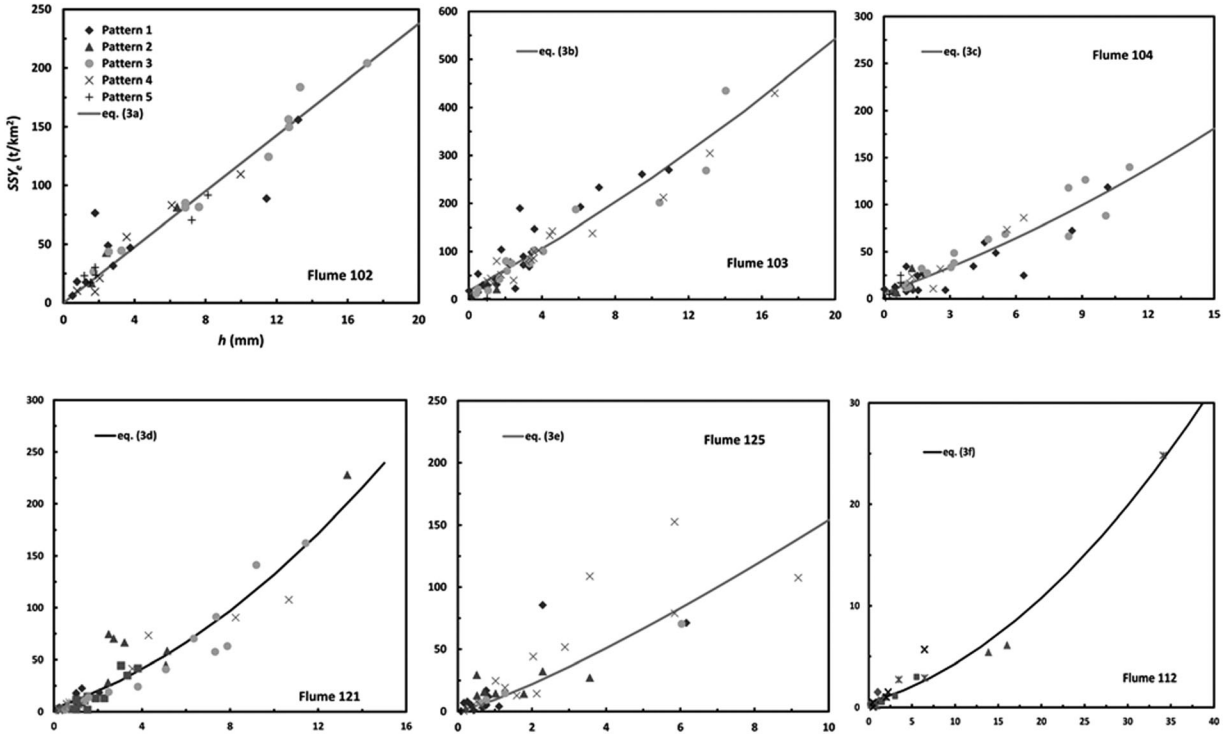

Figure 7. The relationships between event specific sediment yield (SSY_e) and runoff depth (h) for the six watersheds at the unit-source scale.

$$\text{Flume 102} \quad SSY_e = 0.100h^2 + 9.48h + 11.42 \quad r^2 = 0.92 \tag{3a}$$

$$\text{Flume 103} \quad SSY_e = 0.273h^2 + 20.78h + 17.86 \quad r^2 = 0.93 \tag{3b}$$

$$\text{Flume 104} \quad SSY_e = 0.216h^2 + 8.41h + 6.29 \quad r^2 = 0.86 \tag{3c}$$

$$\text{Flume 121} \quad SSY_e = 0.575h^2 + 7.11h + 3.24 \quad r^2 = 0.88 \tag{3d}$$

$$\text{Flume 125} \quad SSY_e = 1.176h^2 + 21.76h – 2.50 \quad r^2 = 0.77 \tag{3e}$$

$$\text{Flume 112} \quad SSY_e = 0.013h^2 - 0.252h + 0.447 \quad r^2 = 0.97 \tag{3f}$$

[27] All equations were statistically significant. Thus, in each watershed, the differences of sediment transport among individual events demonstrated by their different transport patterns were overweighed by the consistent cumulative effect of sediment transport at the event temporal scale. The SSY_e in each watershed can be generally determined by h using the established statistical equations. It should be noted that each watershed had some events (ranging from 2 to 6) that did not fit the developed statistical equations. The number of such events was much less than those forming the trends and thus may be reasonably regarded as outliers. These outliers could be caused by possible sampling failure or some random abnormal transport processes and did not have significant impact on the long-term trend of event-based sediment transport.

3.3. Watersheds at the Large Spatial Scale

[28] The recorded events can also be classified into the same five patterns as those in the previous two spatial scales. Perhaps because the number of events recorded in Flumes 3, 4, 7, and 8 were less than 10 in each case, these events fell into only some of the five patterns (Table 1). Yet, in each watershed at this spatial scale, no single statistically significant sediment rating curve was available for all instantaneous pairs of SSC and Q (Figure 3c). This suggests that with the dominance of in-channel hydraulic transport processes, suspended sediment transport was still complex at the intraevent scale. In other words, the increase of spatial scale did not reduce the degree of complexity for suspended sediment transport at the intraevent temporal scale.

[29] Again, at the event temporal scale, points from different patterns collapsed to single trends in terms of the SSY_e-h relationship, which may be characterized by a statistically significant power function in each watershed:

$$\text{Flume 1} \quad SSY_e = 26.05h^{1.05} \quad r^2 = 0.957 \tag{4a}$$

$$\text{Flume 2} \quad SSY_e = 18.60h^{1.07} \quad r^2 = 0.897 \tag{4b}$$

$$\text{Flume 3} \quad SSY_e = 14.63h^{1.13} \quad r^2 = 0.987 \tag{4c}$$

$$\text{Flume 4} \quad SSY_e = 9.50h^{1.21} \quad r^2 = 0.995 \tag{4d}$$

$$\text{Flume 6} \quad SSY_e = 16.81h^{1.08} \quad r^2 = 0.995 \tag{4e}$$

$$\text{Flume 7} \quad SSY_e = 16.02h^{1.31} \quad r^2 = 0.998 \tag{4f}$$

$$\text{Flume 8} \quad SSY_e = 28.05h^{0.98} \quad r^2 = 0.966 \qquad (4g)$$

$$\text{Flume 11} \quad SSY_e = 20.31h^{0.86} \quad r^2 = 0.932 \qquad (4h)$$

[30] In Flume 1, one event from both patterns one and three had discernibly higher SSY_e values than predicted by equation (4a) (Figure 8a). In Flume 2, two events from both patterns two and three had discernibly higher SSY_e values than predicted by equation (4b) (Figure 8b). In Flume 6, several events had relatively higher SSY_e values than predicted by equation (4e) (Figure 8e). However, these inconsistent events bear limited influence on the overall trends of the events, highlighting their role as relatively random events rather than a part of the general trend. The very high r^2 values in other flumes with no obvious inconsistent events (Figures 8c–8h) indicated that their event-based data had strong trends that can be quantified by the associated statistical equations.

4. Discussion

4.1. Intraevent Variations of Suspended Sediment Transport

[31] The fact that no single sediment rating curve is capable of characterizing the relationship between *SSC* and *Q* for watersheds at any of the three spatial scales indicates that suspended sediment transport over multiple spatial scales is not solely controlled by *Q*. Hydraulically, this is because suspended sediment is transported below capacity [*Walling*, 1977], which is caused by variable sediment supply and heterogeneous sediment sizes. Types of hysteresis loops may imply possible sources of sediment supply such as we have described in section 3.1.1. However, hysteresis analysis fails to reveal the specific mechanisms causing a given type of hysteresis loop even for events of the same pattern. For example, the anticlockwise loops associated with the pattern-three events at all three spatial scales suggest that these events had either ample sediment supply or additional sediment input during the falling limb of the events, but one cannot determine which factor was active and what geomorphological processes led to the true cause. As the spatial scale increases from the plot to the unit-source and further to the large scales, not only in-channel incision and bank erosion, but also watershed mean slope and mean length may serve as additional sediment sources [*Harrison*, 2000]. Consequently, though events of the same pattern have the same hysteresis loop, the loop of each event may have resulted from different combinations of possible sediment sources. Therefore, hysteresis analysis remains a qualitative tool providing insufficient information of possible sediment sources. Quantitative determination of variable sediment sources during a given storm event calls for new process-based approaches. One of these is characterizing various hydrological and sediment connectivity between all possible sediment sources and downstream sediment transport of a watershed [*Wainwright et al*., 2011]. Specific sediment-transport processes and the associated paths may be elucidated using detailed data obtained from field monitoring and watershed models identifying diverse soil erosion processes [*Mueller et al*., 2008; *Turnbull et al*., 2010]. Another approach is directly identifying a variety of potential sediment sources using benthic diatom, geochemical or radionuclide tracers coupled with event-based *Q* and *SSC* measurements [*Collins et al*., 1997; *Pfister et al*., 2009; *Wilson et al*., 2012].

4.1. A General Model

[32] At the event temporal scale, regression analysis gave rise to two different types of best-fit SSY_e-*h* relationships at different spatial scales: the second-order polynomial equation at the plot and unit-source watersheds, and the power equation at the large scale. To understand the

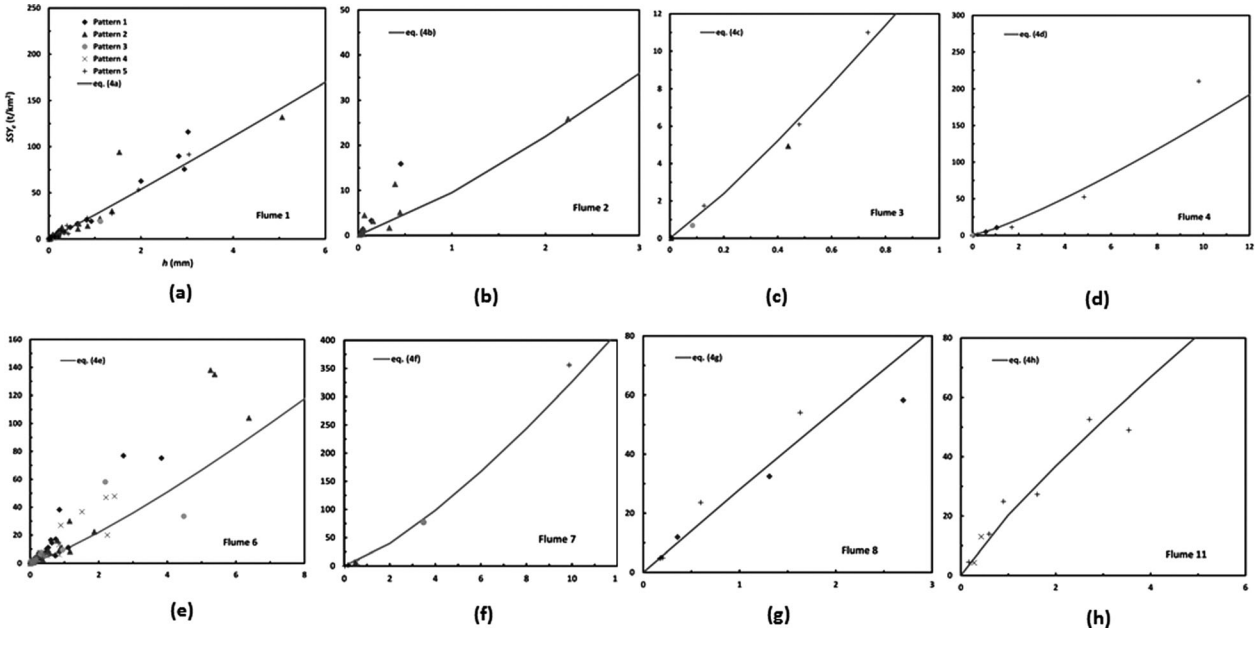

Figure 8. The relationships between event specific sediment yield (SSY_e) and runoff depth (*h*) for the eight watersheds at the large scale.

difference, we compared the outcomes of regression analysis using four different functions, second-order polynomial, power, linear with an intercept, and proportional functions. These outcomes indicated that for all watersheds, the SSY_e-h relationship may be generally characterized by a simple proportional equation,

$$SSY_e = nh \tag{5}$$

where n is a constant, which has the same unit as the suspended sediment concentration (kg/m^3) and may be different in different watersheds (Table 2). In the plot-scale watersheds, r^2 value of equation (5) for Flume 105 was very close to that of equation (1) and for Flume 106 was the same as that of equation (2). Comparing the sum of SSY_e for all measured events in Flume 105 with that predicted by equation (1) and by equation (5) gave percent of predictive error of 0.01% (i.e., $\%E_b$ in Table 2) and 12.0% (i.e., $\%E_p$ in Table 2), respectively. Given that sediment load in Walnut Gulch is highly variable, the predictive error of 12.0% by equation (5) was considered acceptable, though it is higher than that produced by equation (1). For Flume 106, $\%E_p$ was −2.99%, which is very similar to $\%E_b$ (i.e., 1.64%) (Table 2). Thus, equation (5) can reasonably well replace equations (1) and (2) in characterizing the event-based processes of suspended sediment transport in watersheds at the plot scale.

[33] In the unit-source watersheds, r^2 values varied from 0.711 to 0.905 when the data of SSY_e and h from each watershed were fitted by equation (5) (Table 2). These r^2 values were statistically significant and comparable with those for the polynomial equations (i.e., equations (3a)–(3f). Although values of $\%E_b$ were generally less than $\%E_p$ for all watersheds at this spatial scale, values of $\%E_p$ were generally limited to less than 9% (Table 2). These results suggest that equation (5) is a statistically significant and physically reasonable mathematical model for characterizing in general the cumulative effect of event suspended sediment transport for all unit-source watersheds. At the large scale, fitting the SSY_e-h relationship by equation (5) led to similarly high r^2 values for all watersheds to those associated with the power equations (i.e., equations (4a)–(4h)) except in Flume 11 where $\%E_p$ (−10.15%) was much higher than $\%E_b$ (0.80%). However, about 10% of underestimation of SSY_e using equation (5) is a limited error for sediment-load determination. Thus, equation (5) also serves as an equivalent function to equations (4a)–(4h) in predicting SSY_e values of watersheds at this spatial scale.

[34] Overall, equation (5) can replace the polynomial equations at the plot and unit-source scales and the power equations at the large scale to reasonably well predict event sediment yields in all watersheds of the study area. Thus, it is indeed a general model for characterizing event-based suspended sediment transport in all watersheds. This finding is consistent with the result from the dry, loess area of northwestern China in which event-based suspended sediment can be characterized by the proportional model [*Zheng et al*., 2008, 2011]. The existence of this general model suggests that though the complex transport processes during a given storm event are very difficult to quantify, their synoptic effect over the event can be simply captured by a proportional relationship between SSY_e and h.

Table 2. The Proportional Model, Its Statistical Significance, and Comparison Between the Proportional Model and Best Empirical Equations for All Selected Watersheds

Watersheds	A (km^2)	n (kg/m^3)	r^2	$\%E_b$[a]	$\%E_p$[b]
The plot scale					
Flume 105	0.0018	3.64	0.720	−0.01	12.0
Flume 106	0.0034	3.43	0.800	1.64	−2.99
The unit-source scale					
Flume 102	0.0146	11.88	0.905	0.47	−4.90
Flume 103	0.0368	27.00	0.923	0.01	−4.48
Flume 104	0.0453	11.16	0.853	0.02	−5.71
Flume 121	0.0542	12.59	0.859	−0.02	6.88
Flume 125	0.0591	16.27	0.711	−9.6	−13
Flume 112	0.0186	0.632	0.926	−0.62	8.62
The large scale					
Flume 1	149.33	29.08	0.919	−6.23	3.15
Flume 2	113.72	21.87	0.787	8.79	−22.5
Flume 3	8.98	13.64	0.976	1.59	4.47
Flume 4	2.27	18.95	0.927	−14.52	18.54
Flume 6	95.1	19.37	0.862	−5.61	3.59
Flume 7	13.52	34.39	0.978	−6.33	12.14
Flume 8	15.5	25.24	0.898	2.21	−7.47
Flume 11	8.24	16.65	0.874	0.80	−10.15

[a]The percent error between the sums of measured and predicted SSY_e using the best-fit equations.

[b]The percent error between the sums of measured and predicted SSY_e using equation (5).

4.3. Implication of the General Model

[35] Mathematically, the general model, which is expressed in the form of equation (5), indicates that SSY_e is proportional to h by a constant n. The physical meaning of n may be revealed by reviewing the mathematical expressions of SSY_e and h as follows.

[36] Suspended sediment load, Q_s is defined as

$$Q_s = a\sum_{i=1}^{n} Q_i C_i t_i \tag{6}$$

where Q_i and C_i are the water discharge and sediment concentration measured at time i and a is the unit conversion factor. Event specific suspended sediment yield, SSY_e is defined as

$$SSY_e = \frac{Q_s}{A} = Q_s/A = a\sum_{i=1}^{n} Q_i C_i t_i/A \tag{7}$$

where A is the area of a watershed. In addition, the total volume of water during a given rainfall event by definition may be written

$$V = \sum_{i=1}^{n} Q_i t_i \tag{8}$$

[37] Thus, runoff depth, h can be generally displayed as

$$h = \frac{V}{A} = \frac{\sum_{i=1}^{n} Q_i t_i}{A} \tag{9}$$

[38] It follows that the ratio of SSY_e to h, which is denoted as m, may be expressed as

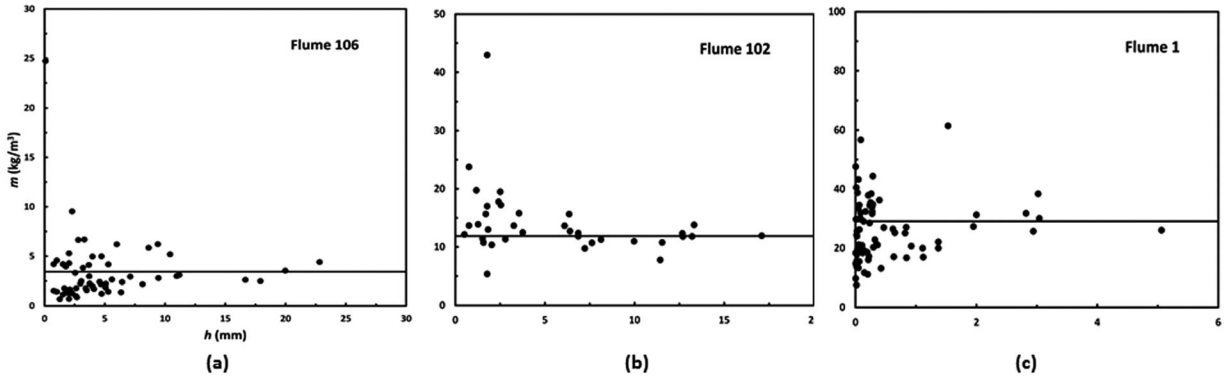

Figure 9. Examples of the relationships between volume-weighted mean sediment concentration (m) and runoff depth (h) at the three spatial scales. (a) The plot scale; (b) the unit-source scale; (c) the large scale.

$$m = \frac{SSY_e}{h} = \frac{a\sum_{i=1}^{n} Q_i C_i t_i}{\sum_{i=1}^{n} Q_i t_i} = a\frac{C_1 V_1 + C_2 V_2 + \cdots + C_n V_n}{V} = a\sum_{i=1}^{n} C_i F_i \quad (10)$$

where $F_i = V_i/V$. So, m is the volume-weighted mean sediment concentration.

[39] If $t_1 = t_2 = \ldots\ t_n$, then,

$$m = \frac{SSY_e}{h} = a\frac{\sum_{i=1}^{n} Q_i C_i}{\sum_{i=1}^{n} Q_i} = \frac{aC_1 Q_1 + C_2 Q_2 + \cdots + C_n Q_n}{\sum_{i=1}^{n} Q_i} = a\frac{C_1 Q_1 + C_2 Q_2 + \cdots + C_n Q_n}{Q_t} = a\sum_{i=1}^{n} C_i f_i \quad (11)$$

where $f_i = Q_i/Q_t$. Thus, m becomes the discharge-weighted mean sediment concentration.

[40] Equations (6)–(11) show that the volume-weighted mean concentration, m_i, which represents average amount of suspended sediment transported over an event, i, may be calculated as the ratio of the associated $SSYe_i$, to h_i. However, m_i calculated in this way is different from the constant n in equation (5), which is obtained by regressing all $SSYe_i$ against all h_i values. For a given watershed, though m_i varies from event to event, n remains constant over all events, suggesting that n is the characteristic volume-weighted concentration of the watershed regardless of the event difference both in magnitude and intensity. In watersheds at all three spatial scales, the degree of variation of m_i decreases as h increases (Figures 9a–9c), suggesting that with the increase of h (and hence the size of rainfall event, either in magnitude or intensity or both), the significant impact of rainfall intensity through rain splash and soil detachment gives way to the dominance of sediment-transport process due to the increase of overland flow and then the processes due to augmented in-stream hydraulics. Also shown in Figure 9 is that n is always consistent with the trend of m_i for large events. During these events, surface runoff on hillslopes and in-stream flows are more hydrologically connected and thus, sediment exported out of a watershed reflects overall ability of soil erosion and sediment transport of the entire watershed, which reflects the coupled effect of morphology, land cover/use, and soil properties of a watershed on sediment transport.

[41] The implication of the general model is that for a given watershed, though the volume-weighted suspended sediment concentration (i.e., m_i) varies from event to event due to the variable storm intensities and durations, these concentrations can be simply represented by a constant n for all events. In other words, at the event time scale, the synoptic effect of complex sediment-transport processes for each watershed may be described by the characteristic volume-weighted suspended sediment concentration, n. For example, values of n for watersheds in the study area range from 0.63 to 34.69 kg/m^3 (Table 2) whereas those for watersheds in the loess area of northwestern China are from 485 to 941 kg/m^3 [*Zheng et al*., 2012]. The obvious difference between n values in two regions reflects their distinct characteristics of sediment transport: in the former, flows transport sediment of variable, but limited high concentrations whereas in the latter, flows transported hyperconcentrated sediment.

4.3. The Unique Behavior of Flume 112

[42] At the unit-source spatial scale, n value of Flume 112 is significantly less than those of other watersheds (Table 2). Evidently, the processes of suspended sediment transport in this watershed were different from those in others. The most discernible difference between this watershed and others is vegetation cover: Flume 112 is dominated by grass lands while others are dominated by shrub lands. Because many studies on Walnut Gulch have shown [*Parsons et al*., 1996; *Turnbull et al*., 2010; *Wainwright et al*., 2000] that erosion rates are higher in shrub lands than in grass lands, it is readily to solely attribute such transport difference to the vegetation difference. However, *Nearing et al*. [2005] discovered that at the vegetation patch scale, erosion rates in a grassland watershed are indeed close to those in a shrub land watershed, though sediment yield from the entire watershed is much lower in the former. The relatively high erosion rates at the much smaller spatial scale of the grassland watershed is mainly caused by relatively small surface roughness due to less cover of rock fragments. Nonetheless, these high erosion rates did not turn into equivalently high sediment-transport

rates at the entire watershed scale because of poor hydrological connectivity among small plots and more importantly, a swale located above the sampling site of Flume 112 forming a local topographic sink.

[43] Therefore, the special topographical structure appears to be the primary cause for the low n value in Flume 112, which may be further supported by comparing the data used in Figure 7 with those collected in 2006. Because of the unusual dry weather, vegetation cover was reduced significantly in that year. Thus, the impact of vegetation on flow resistance and hydrological connectivity was attenuated to a large degree in 2006, causing significantly higher suspended sediment transport [*Polyakov et al.*, 2010]. The increased transport ability was well represented by the significantly high n value in 2006 than that in other years (Figure 10). However, the n value associated with the data in 2006 was only 4.33 kg/m^3, still much less than those of other watersheds at the unit-source spatial scale.

4.4. The Spatial Variation of n Values

[44] In all other watersheds with the same dominant vegetation cover (i.e., shrub lands), watersheds at the large scale have a wide range of areas (from 2 to 149 km^2). Spatially, they involve two nested sequences (see Figure 1) whose n values were plotted against their areas (Figure 11). For both sequences, as the watershed area increased, values of n changed, but did not show any significant trend. It became more obvious when these n values were combined with those of the remaining shrub land watersheds and were plotted against their sizes (Figure 12). For watersheds greater than 0.01 km^2, n varied within a constrained range from 11.16 to 34.49 kg/m^3 with the mean of 19.40 kg/m^3 (solid squares and triangles in Figure 12). The n values for the two smaller watersheds with $A < 0.01$ km^2 were less, suggesting at the plot scale suspended sediment transport dominated by hillslope erosion processes due to overland flows [*Lane et al.*, 1997] is limited. For watersheds with areas greater than this threshold value, in-channel transport process becomes more and more important. The fact that n centers around a constant value (i.e., 19.40 kg/m^3) means that n approximately remains unchanged as watershed area

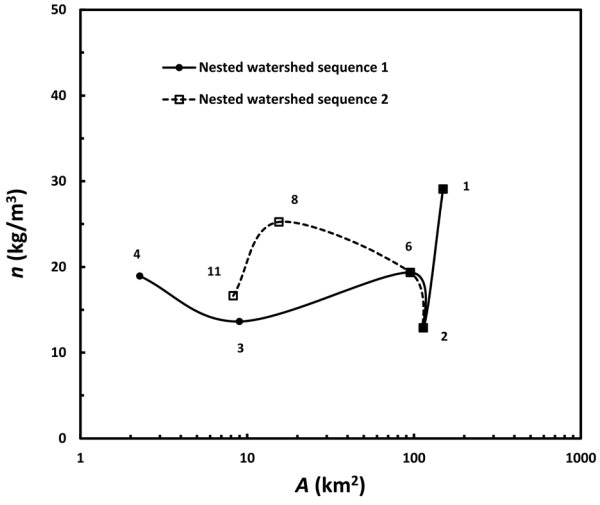

Figure 11. Values of n in two sets of nested watersheds at the large scale (the number next to the symbol represents the associated watershed).

increases from 0.01 to about 150 km^2. To further validate this trend, we compiled more data collected from different watersheds of Walnut Gulch. These data were obtained from watersheds that have areas that mostly fall between those of unit-source and large watersheds [*Lane et al.*, 1997]. Since the reported annual sediment yields of these watersheds were averages of cumulative sediment yields over multiple years, n values calculated for these watersheds are not exactly equivalent to those calculated using equation (5). Nonetheless, the calculated n values generally follow the same trend (Figure 12), suggesting that the approximately constant n value prevails in watersheds with areas ranging from 0.01 to about 150 km^2.

[45] The implication is that at the event time scale, the processes of suspended sediment transport are similar in watersheds of any size that are greater than 0.01 km^2. This finding is at odds with current consensus that suspended sediment transport varies significantly as watershed area increases in Walnut Gulch partially because of the nonlinearity of runoff

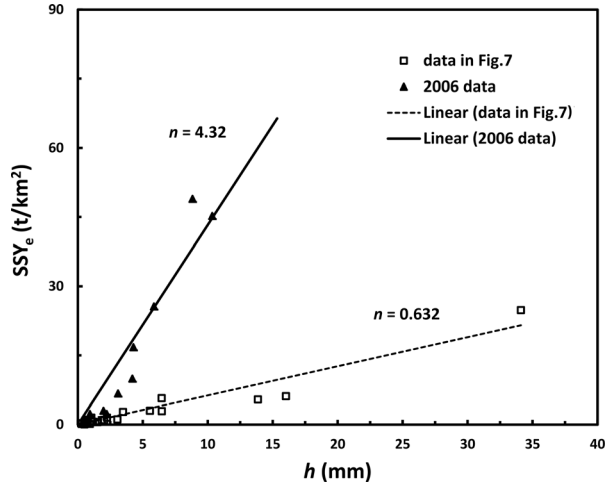

Figure 10. Impact of vegetation on suspended sediment transport in Flume 112.

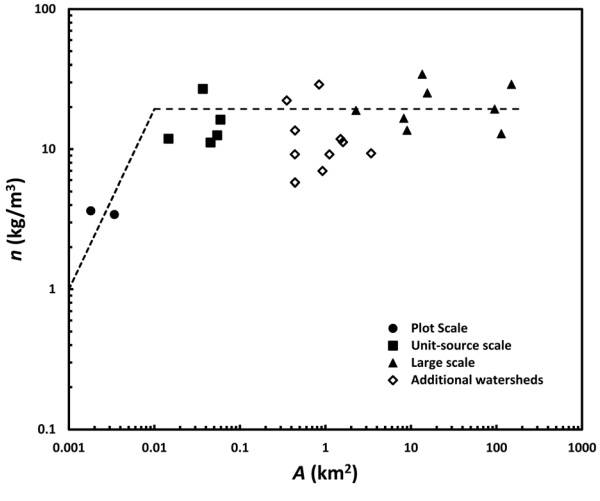

Figure 12. Spatial variations of n values over three spatial scales.

response as watershed area increases [*Goodrich et al*., 1997]. In practice, the approximately constant n value allow us to study the long-term trends of sediment yields in large-scale watersheds based on collected discharge data, which is relatively easy to handle.

5. Conclusions

[46] We studied the spatial and temporal variations of suspended sediment transport in Walnut Gulch of southeastern Arizona using event-based long-term data compiled from 16 watersheds of variable sizes. At the intraevent temporal scale, the identified five transport patterns existed in watersheds at all spatial scales, confirming the assertion that sediment transport in semiarid environments is highly variable. However, these patterns have limited capacity to characterize the processes of suspended sediment transport because even within the same pattern, transport processes may be dramatically different (Figure 3). At this temporal scale, predicting instantaneous suspended sediment concentrations or transport rates becomes unreliable because a specific concentration or rate is the outcome of interaction among rainfall, vegetation cover, soil, and topography. Research focus should be on identifying the relative importance of relevant processes in the context of hydrological and sediment-transport connectivity [*Wainwright et al*., 2011].

[47] At the event temporal scale, suspended sediment transport with all five patterns can be generally described by a statistically significant and well-fit empirical equation between event specific sediment yield (SSY_e) and event runoff depth (h) for all selected watersheds, indicating a reduced complexity in suspended sediment transport at this temporal scale regardless of spatial variations. Furthermore, we discovered that the SSY_e-h relationship can be statistically well described using a general proportional model $SSY_e = nh$, where n is a constant with the unit of kg/m^3 and is conceptually equivalent to the volume-weighted event mean sediment concentration. This implies that though event sediment yield of a watershed in Walnut Gulch varies from storm to storm, the ability of transporting suspended sediment by the watershed is quantitatively characterized by the value of n irrespective of storm intensity and duration, and watershed sizes. The higher the n value, the more sediment can be exported from a watershed. Thus, n is a new sediment index that can quantitatively determine the degree of sediment loss from a watershed. Under a similar storm, a watershed with a higher n value must experience more sediment loss than that with a lower n value. This is potentially a useful tool for monitoring the long-term effect of global warming and land use changes on sediment transport with more observed data. The change of n value in the future will indicate whether sediment transport will be accelerated or decelerated.

[48] The significant low n value for Flume 112 compared to those of other watersheds with similar sizes suggests that Flume 112 has different processes of suspended sediment transport than other similar-sized watersheds in this area. Although the low n value may be attributed to different vegetation cover, geomorphological connectivity, and sampling methods between Flume 112 and other similar-sized watersheds, the topographic sink (i.e., swale) in this watershed is the main culprit.

[49] Over the three spatial scales (i.e., the plot, unit-source, and large scales), n values showed a threshold behavior: they followed a positively increasing trend with watershed area (A) for $A < 0.01$ km^2 and remained roughly constant for $A > 0.01$ km^2. In the former watersheds, suspended sediment transport is predominately controlled by hillslope hydrological and erosion processes, while in the latter, sediment transport is controlled by both hillslope and in-stream processes. The constant trend of n values for large watersheds is particularly important. This trend suggests that the ability of transporting sediment quantified by the n value is independent of watershed area. Thus, n can better represent the nature of sediment transport in a watershed than the specific sediment yield, which changes with the watershed area in a complicated fashion [*de Vente et al*., 2007; *Parsons et al*., 2006; *Walling*, 1983].

References

Achite, M., and S. Ouillon (2007), Suspended sediment transport in a semiarid watershed, Wadi Abd, Algeria (1973–1995), *J. Hydrol.*, *343*, 187–202.

Alexandrov, Y., J. B. Laronne, and I. Reid (2007), Intra-event and interseasonal behaviour of suspended sediment in flash floods of the semiarid northern Negev, Israel, *Geomorphology*, *85*, 85–97.

Alexandrov, Y., J. B. Laronne, I. Reid, and H. Cohen (2009), Suspended sediment load, bed load, and dissolved load yields from a semiarid drainage basin: A 15-year study, *Water Resour. Res.*, *45*, W08408, doi: 10.1029/02008WR007314.

Bisantino, T., F. Gentile, and G. T. Liuzzi (2011), Continuous monitoring of suspended sediment load in semi-arid environments, in *Sediment Transport*, chap. 15, edited by S. S. Ginsberg, doi:10.5772/15373.

Collins, A. L., D. E. Walling, and J. G. L. Leeks (1997), Fingerprinting the origin of fluvial suspended sediment in larger river basins: Combining assessment of spatial provenance and source type, *Geogr. Ann. Ser. A*, *79*, 239–254.

Coppus, R., and A. C. Imeson (2002), Extreme events controlling erosion and sediment transport in a semi-arid sub-Andean valley, *Earth Surf. Processes Landforms*, *27*, 1365–1375.

de Vente, J., J. Poesen, M. Arabkhedri, and G. Verstraeten (2007), The sediment delivery problem revisited, *Prog. Phys. Geogr.*, *31*(2), 155–178.

Fang, H. Y., Q. G. Cai, H. Chen, and Q. Y. Li (2008), Temporal changes in suspended sediment transport in a gullied loess basin: The lower Chabagou Creek on the Loess Plateau in China, *Earth Surf. Processes Landforms*, *33*, 1977–1992.

Gao, P. (2008), Understanding watershed suspended sediment transport, *Prog. Phys. Geogr.*, *32*, 243–263.

Gao, P., and M. Josefson (2012), Suspended sediment dynamics during hydrological events in a central New York watershed, *Geomorphology*, *139–140*, 425–437.

Gentile, F., T. Bisantino, R. Corbino, F. Milillo, G. Romano, and G. Trisorio Liuzzi (2010), Monitoring and analysis of suspended sediment transport dynamics in the Carapelle torrent (Southern Italy), *Catena*, *80*, 1–8.

Goodrich, D. C., L. J. Lane, R. M. Shillito, and S. N. Miller (1997), Linearity of basin response as a function of scale in a semiarid watershed, *Water Resour. Res.*, *33*(12), 2951–2965.

Goodrich, D. C., T. O. Keefer, C. L. Unkrich, M. H. Nichols, H. B. Osborn, J. J. Stone, and J. R. Smith (2008), Long-term precipitation database, Walnut Gulch Experimental Watershed, Arizona, United States, *Water Resour. Res.*, *44*, W05S04, doi:10.1029/2006WR005782.

Harrison, C. G. A. (2000), What factors control mechanical erosion rates?, *Int. J. Earth Sci.*, *88*, 752–763.

Issa, O. M., Y. L. Bissonnais, O. Planchon, D. Favis-Mortlock, N. Silvera, and J. Wainwright (2006), Soil detachment and transport on field- and laboratory-scale interrill areas: Erosion processes and the size-selectivity of eroded sediment, *Earth Surf. Processes Landforms*, *31*, 929–939.

Jansson, M. B. (2002), Determining sediment source areas in a tropical river basin, *Costa Rica, Catena*, *47*, 63–84.

Kincaid, D. R., H. B. Osborne, and J. L. Gardner (1966), Use of unit source watersheds for hydrological investigations in the semi-arid southwest, *Water Resour. Res.*, *2*(2), 381–392.

Lane, L. J., M. Hernandez, and M. Nichols (1997), Processes controlling sediment yield from watersheds as functions of spatial scale, *Environ. Model. Software*, *12*(4), 355–369.

Langlois, J. L., D. W. Johnson, and G. R. Mehuys (2005), Suspended sediment dynamics associated with snowmelt runoff in a small mountain stream of Lake Tahoe (Nevada), *Hydrol. Processes*, *19*, 3569–3580.

Lefrancois, J., C. Grimaldi, C. Gascuel-Odoux, and N. Gilliet (2007), Suspended sediment and discharge relationships to identify bank degradation as a main sediment source on small agricultural catchments, *Hydrol. Processes*, *21*, 2923–2933.

López-Tarazón, J. A., R. J. Batalla, D. Vericat, and J. C. Balasch (2010), Rainfall, runoff and sediment transport relations in a mesoscale mountainous catchment: The River Isábena (Ebro basin), *Catena*, *82*, 23–34.

Martinez-Mena, M. V., V. Castillo, and J. Albaladejo (2001), Hydrological and erosional response to natural rainfall in a semi-arid area of south-east Spain, *Hydrol. Processes*, *15*, 557–571.

Moran, M. S., D. P. C. Peters, M. P. McClaran, M. H. Nichols, and M. A. Adams (2008), Long-term data collection at USDA experimental sites for studies of ecohydrology, *Ecohydrology*, *1*, 377–393.

Mueller, E. N., J. Wainwright, and A. J. Parsons (2008), Spatial variability of soil and nutrient characteristics of semi-arid grasslands and shrublands, Jornada Basin, New Mexico, *Ecohydrology*, *1*, 3–12.

Mulligan, M. (1998), Modeling the geomorphological impact of climatic variability and extreme events in a semiarid environment, *Geomorphology*, *24*, 59–78.

Nearing, M. A., A. Kimoto, and M. H. Nichols (2005), Spatial patterns of soil erosion and deposition in two small, semiarid watersheds, *J. Geophys. Res.*, *110*, F04020, doi:10.1029/02005JF000290.

Nearing, M. A., M. H. Nichols, J. J. Stone, K. G. Renard, and J. R. Simanton (2007), Sediment yields from unit-source semiarid watersheds at Walnut Gulch, *Water Resour. Res.*, *43*, W06426, doi:10.1029/02006WR005692.

Nichols, M. H. (2006), Measured sediment yield rates from semiarid rangeland watersheds, *Rangeland Ecol. Manage.*, *59*, 55–62.

Nichols, M. H., and E. Anson (2008), Southwest Watershed Research Center Data Access Project, *Water Resour. Res.*, *44*, W05S03, doi:10.1029/2006WR005665.

Nichols, M. H., J. J. Stone, and M. A. Nearing (2008), Sediment database, Walnut Gulch Experimental Watershed, Arizona, United States, *Water Resour. Res.*, *44*, W05S06, doi:10.1029/2006WR005682.

Oeurng, C., S. Sauvage, and J. Sánchez-Pérez (2010), Dynamics of suspended sediment transport and yield in a large agricultural catchment, southwest France, *Earth Surf. Processes Landforms*, *35*, 1289–1301, doi:1210.1002/esp.1971.

Osterkamp, W. R. (2008), Geology, soils, and geomorphology of the Walnut Gulch experimental watershed, tombstone, Arizona, *J. Ariz. Nev. Acad. Sci.*, *40*(2), 136–154.

Parsons, A. J., A. D. Abrahams, and S.-H. Luk (1991), Size characteristics of sediment in interrill overland flow on a semiarid hillslope, Southern Arizona, *Earth Surf. Processes Landforms*, *16*, 143–152.

Parsons, A. J., A. D. Abrahams, and J. Wainwright (1996), Responses of interrill runoff and erosion rates to vegetation change in Southern Arizona, *Geomorphology*, *14*, 311–317.

Parsons, A. J., R. E. Brazier, J. Wainwright, and D. M. Powell (2006), Scale relationships in hillslope runoff and erosion, *Earth Surf. Processes Landforms*, *31*, 1384–1393.

Pfister, L., J. J. McDonnell, S. Wrede, D. Hlubikova, P. Matgen, F. Fenicia, L. Ector, and L. Hoffmann (2009), The rivers are alive: On the potential for diatoms as a tracer of water source and hydrological connectivity, *Hydrol. Processes*, *23*, 2841–2845.

Polyakov, V. O., M. A. Nearing, J. J. Stone, E. P. Hamerlynck, M. H. Nichols, C. D. H. Collins, and R. L. Scott (2010), Runoff and erosional responses to a drought-induced shift in a desert grassland community composition, *J. Geophys. Res.*, *115*, G04027 doi:10.1029/02010JG001386.

Reid, I., J. B. Laronne, D. M. Powell, and C. Garcia (1994), Flash floods in desert ephemeral rivers, *EOS*, *75*(39), 452–453.

Romkens, M. J., S. N. Prasa, and F. D. Whisler (1990), Surface sealing and infiltration, in *Hillslope Hydrology*, edited by M. G. Anderson and T. P. Burt, pp. 127–172, Wiley, New York.

Sadeghi, S. H. R., T. Mizuyama, S. Miyata, T. Gomi, K. Kosugi, T. Fukushima, S. Mizugaki, and Y. Onda (2008), Development, evaluation and interpretation of sediment rating curves for a Japanese small mountainous reforested watershed, *Geoderma*, *144*(1–2), 198–211.

Seeger, M., M.-P. Erreab, S. Beguerí, J. Arnáez, C. Martí, and J. M. García-Ruiz (2004), Catchment soil moisture and rainfall characteristics as determinant factors for discharge/suspended sediment hysteretic loops in a small headwater catchment in the Spanish Pyrenees, *J. Hydrol.*, *288*, 299–311.

Simanton, J. R., W. R. Osterkamp, and K. G. Renard (1993), Sediment yield in a semiarid basin: Sampling equipment impacts, *IAHS Publ.*, *217*, 3–9.

Smith, H. G., and D. Dragovich (2009), Interpreting sediment delivery processes using suspended sediment-discharge hysteresis patterns from nested upland catchments, south-eastern Australia, *Hydrol. Processes*, *23*, 2415–2426.

Thomas, J. T., N. R. Iverson, M. R. Burkart, and L. A. Kramer (2004), Longterm growth of a valley-bottom gully, western Iowa, *Earth Surf. Processes Landforms*, *29*, 995–1009.

Turnbull, L., J. Wainwright, and R. E. Brazier (2010), Changes in hydrology and erosion over a transition from grassland to shrubland, *Hydrol. Processes*, *24*, 393–414.

Wainwright, J., A. J. Parsons, and A. D. Abrahams (2000), Plot-scale studies of vegetation, overland flow and erosion interactions: Case studies from Arizona and New Mexico, *Hydrol. Processes*, *14*, 2921–2943.

Wainwright, J., L. Turnbull, T. G. Ibrahim, I. Lexartza-Artza, S. F. Thornton, and R. Brazier (2011), Linking environmental regimes, space and time: Interpretations of structural and functional connectivity, *Geomorphology*, *126*, 387–404.

Walling, D. E. (1977), Limitations of the rating curve technique for estimating suspended sediment loads, with particular reference to British rivers, *IAHS Publ.*, *122*, 34–47.

Walling, D. E. (1983), The sediment delivery problem, *J. Hydrol.*, *65*, 209–237.

Williams, G. P. (1989), Sediment concentration versus water discharge during single hydrologic events in rivers, *J. Hydrol.*, *111*, 89–106.

Wilson, C. G., A. N. T. Papanicolaou, and K. D. Denn (2012), Partitioning fine sediment loads in a headwater system with intensive agriculture, *J. Soils Sediments*, *12*, 966–981.

Zheng, M. G., Q. G. Cai, and Q. J. Cheng (2008), Modelling the runoff-sediment yield relationship using a proportional function in hilly areas of the Loess Plateau, North China, *Geomorphology*, *93*, 288–301.

Zheng, M. G., F. Qin, L. Y. Sun, D. L. Qi, and Q. G. Cai (2011), Spatial scale effects on sediment concentration in runoff during flood events for hilly areas of the Loess Plateau, China, *Earth Surf. Processes Landforms*, *36*, 1499–1509.

Zheng, M. G., J. S. Yang, D. L. Qi, L. Y. Sun, and Q. G. Cai (2012), Flow-sediment relationship as functions of spatial and temporal scales in hilly areas of the Chinese loess plateau, *Catena*, *98*, 29–40.